

Fluorescent Human RAD51 Reveals Multiple Nucleation Sites and Filament Segments Tightly Associated along a Single DNA Molecule

Mauro Modesti,^{1,*} Dejan Ristic,¹ Thijn van der Heijden,³ Cees Dekker,³ Joost van Mameren,⁴ Erwin J.G. Peterman,⁴ Gijs J.L. Wuite,⁴ Roland Kanaar,^{1,2} and Claire Wyman^{1,2}

¹Department of Cell Biology & Genetics

²Department of Radiation Oncology

Erasmus Medical Center, PO Box 2040, 3000 CA Rotterdam, The Netherlands

³Kavli Institute of Nanoscience, Delft University of Technology, Lorentzweg 1, 2628 CJ Delft, The Netherlands

⁴Laser Centre and Department of Physics and Astronomy, Vrije Universiteit, De Boelelaan 1081, 1081 HV, Amsterdam, The Netherlands

*Correspondence: m.modesti@erasmusmc.nl

DOI 10.1016/j.str.2007.04.003

SUMMARY

The DNA strand-exchange reactions defining homologous recombination involve transient, nonuniform allosteric interactions between recombinase proteins and their DNA substrates. To study these mechanistic aspects of homologous recombination, we produced functional fluorescent human RAD51 recombinase and visualized recombinase interactions with single DNA molecules in both static and dynamic conditions. We observe that RAD51 nucleates filament formation at multiple sites on double-stranded DNA. This avid nucleation results in multiple RAD51 filament segments along a DNA molecule. Analysis of fluorescent filament patch size and filament kinks from scanning force microscopy (SFM) images indicate nucleation occurs minimally once every 500 bp. Filament segments did not rearrange along DNA, indicating tight association of the ATP-bound protein. The kinetics of filament disassembly was defined by activating ATP hydrolysis and following individual filaments in real time.

INTRODUCTION

The central event of homologous recombination, exchange of strands between homologous DNA molecules, is catalyzed by recombinase proteins assembled into filaments on DNA. Both single-stranded (ssDNA) and double-stranded DNA (dsDNA) are mandatory substrates for recombinase filaments at different stages of homologous recombination. The mechanism by which recombinase proteins catalyze the DNA rearrangements required for homologous recombination remains elusive despite intense study. It is clear that the dynamic assembly, rear-

angement, and disassembly of recombinase protein filaments are essential elements of DNA strand exchange. Thus, understanding the mechanisms of strand exchange requires defining the dynamic interactions between recombinase proteins and DNA.

Recombinase nucleoprotein filaments are often viewed as regular, continuous, right-handed helices encircling DNA, but several studies indicate a high degree of structural heterogeneity (Conway et al., 2004; Lauder and Kowalczykowski, 1991; Ristic et al., 2005; Shan and Cox, 1996, 1997; van Mameren et al. 2006; Yu et al., 2001). Structural variability indicates that the arrangement of component proteins and DNA is dynamic. This dynamic structure would result from local or transient rearrangements due to binding and disassociation of protein with concomitant DNA extension and relaxation. Recombinase proteins work as catalysts in DNA strand-exchange reactions by coupling nucleotide cofactor binding and hydrolysis to changes in the arrangement of DNA-bound protomers and their turnover. To experimentally probe the dynamic properties of these nucleoprotein filaments, it is necessary to use approaches that allow real-time observation of single molecules or complexes.

For this purpose, we have generated and tested fluorescent variants of the human RAD51 recombinase. Only some fluorescent variants were functionally equivalent to unlabeled protein, emphasizing the care that must be taken to verify function of altered proteins before interpreting their behavior. Filaments assembled on dsDNA reveal that RAD51 nucleates at multiple sites. As a result of this avid nucleation, these RAD51 nucleoprotein filaments were discontinuous and composed of multiple separate filament segments along one DNA molecule. Filaments observed in buffer did not diffuse along DNA, indicating that DNA is tightly associated within RAD51 filaments. In addition, filament disassembly was predictably triggered, observed, and quantified from individual filament segments. These initial observations provide a new view on recombinase filament dynamics that could not be obtained from ensemble measurements.

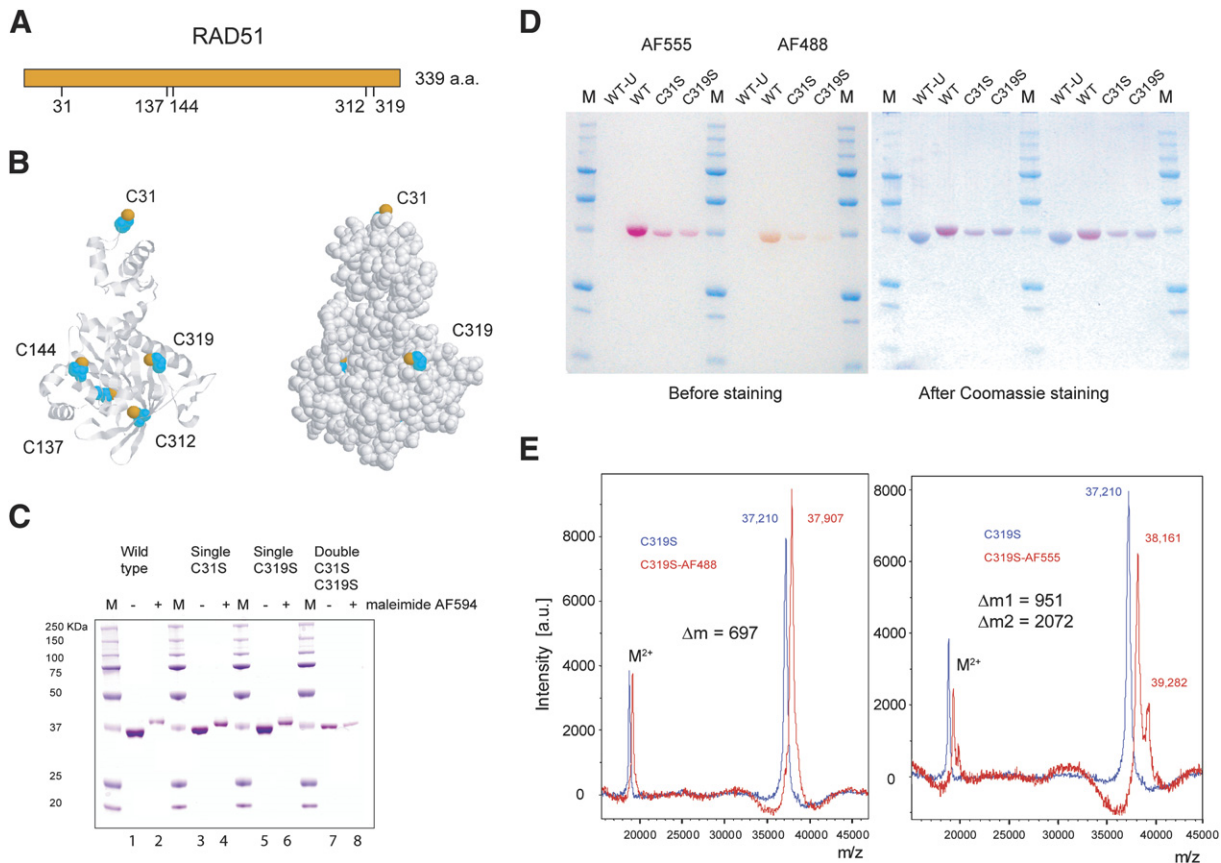


Figure 1. Fluorescent Labeling of Human RAD51

(A) Human RAD51 contains five cysteine residues located at positions 31, 137, 144, 312, and 319. (B) Three-dimensional model of hRAD51 generated by comparison to the known RadA structure (PDB 1T4G) using the 3D-JIGSAW server and displayed with RasMol as a ribbon model (left) and a space-filling model (right). Cysteine residues with their sulfur atom are shown in cyan and orange, respectively. (C) SDS-PAGE and Coomassie staining analysis of wild-type, C31S, C319S, and C31S/C319S RAD51 variants before (–) and after (+) labeling with maleimide Alexa Fluor 594 (AF594). M, size marker. (D) SDS-PAGE analysis of wild-type (WT), C31S, and C319S RAD51 variants labeled with either Alexa Fluor 555 (pink, AF555) or Alexa Fluor 488 (yellow, AF488) before (left) and after brief Coomassie staining (right). WT-U, wild-type unlabeled control. M, size marker as above. (E) Mass spectrometry of the full-length C319S variant before (blue line) and after (red line) labeling with Alexa Fluor 488 (left, AF488) or 555 (right, AF555). M^{2+} , double charged species.

RESULTS AND DISCUSSION

Fluorescent Labeling of RAD51

We labeled human RAD51 with a single fluorophore at a defined position. In contrast to a previously reported strategy (Granéli et al., 2006b), we started with untagged RAD51 and modified it by substitution of one or two native cysteines by serines. The resulting RAD51 variants differ from the wild-type by only one or two atoms. A three-dimensional model of human RAD51, generated by comparative modeling to the known structure of the homologous RadA protein with the 3D-JIGSAW server (<http://www.bmm.icnet.uk/~3djigsaw>) (Bates et al., 2001; Bates and Sternberg, 1999; Contreras-Moreira and Bates, 2002; Wu et al., 2004), indicates that cysteine residues 31 and 319 are accessible to solvent, while cysteine residues 137 and 312 are not, and cysteine residue 144 appears partially buried (see Figures 1A and 1B). Thus, residues

31 and 319 were chosen to couple maleimide-Alexa Fluor dyes to RAD51. Wild-type RAD51, single C31S or C319S, as well as double C31S/C319S variants were produced and labeled with maleimide Alexa Fluor 594. Labeling of the wild-type, C31S, and C319S proteins resulted in retardation of electrophoretic mobility (Figure 1C, compare lanes 1, 3, and 5 to lanes 2, 4, and 6, respectively). The mobility of the C31S/C319S double variant protein was not substantially retarded after treatment (compare lanes 7 and 8), indicating that under the conditions used, C31 and C319 contain the most reactive thiol groups.

The specificity and extent of labeling was tested by mass spectrometry for Alexa Fluor 488- or Alexa Fluor 555-labeled RAD51 variants (Figure 1D). The Alexa Fluor 488-labeled C319S variant shifted 697 Da compared to the unlabeled C319S, corresponding to the incorporation of one molecule of dye per monomer (Figure 1E, left panel; FW of maleimide Alexa Fluor 488 = 720 Da). Quantification

of the peak surface areas indicated that >95% of the sample had one dye/monomer. Similar analysis of RAD51 C319S labeled with Alexa Fluor 555 indicated a mixed population of one, two, or three dyes/monomer in a ratio of ~75%:20%:5%, respectively (Figure 1E, right panel; FW of maleimide Alexa Fluor 555 ~1000 Da). The less bulky Alexa Fluor 488 may facilitate specific single labeling. This dye would be preferred to obtain RAD51 homogeneously labeled with one fluorophore. Consistently, the wild-type protein incorporated mostly two fluorophores per monomer after labeling, and the C31S variant mostly one fluorophore per monomer (data not shown).

One Fluorescent-Labeled RAD51 Variant Is Fully Functional

The variant and labeled proteins were compared to wild-type in several biochemical assays. The critical activities of RAD51 in homologous recombination, strand invasion, and exchange were tested in a D-loop formation assay. The labeled wild-type protein as well as the labeled C31S variant failed to catalyze D-loop formation (Figure 2A). However, the Alexa Fluor 488-labeled C319S variant had activity similar to unlabeled wild-type RAD51 (Figures 2B and 2C). The Alexa Fluor 555-labeled C319S variant had intermediate D-loop activity when compared to wild-type (Figure 2C). ATP hydrolysis activities of C319S variants with and without fluorescent label were similar to unlabeled wild-type RAD51 (Figure 2D). Inactivation of the labeled C31S variant is most likely caused by steric hindrance from the dye attached at position 319 and not the C31S mutation. Unlabeled single variants C31S, C319S, or double variant C31S/C319S were not affected in their ability to catalyze D-loop formation and hydrolyze ATP (Figures 2B and 2C and data not shown). The difference in D-loop formation activity between the Alexa Fluor 488- and 555-labeled C319S variants (Figure 2C) may reflect different dye structure, charge, or attachment stoichiometry (Alexa Fluor 555 is bulkier than Alexa Fluor 488). Alternatively, the length of the carbon linker arm (C5 for 488 and C2 for 555) could influence labeling specificity (see Figure 1E). Based on these standard biochemical assays, RAD51 labeled with Alexa Fluor 488 dye at position 31 was found to be a fully functional recombinase.

The biochemical tests indicated that the Alexa Fluor-labeled RAD51 would form nucleoprotein filaments on DNA, the hallmark structures formed by recombinase proteins. Because multiple protein-protein and protein-DNA interfaces are engaged in nucleoprotein filaments, filament formation is a stringent test for function of the modified RAD51 variants. A previously reported fluorescent RAD51, labeled with Alexa Fluor 555 at nonnative position A11C, is defective in assembling nucleoprotein filaments on DNA (Granéli et al., 2006b; Prasad et al., 2006). Consistent with the results of the D-loop assays, only the Alexa Fluor-labeled C319S variants formed nucleoprotein filaments on dsDNA similar to the wild-type unlabeled protein (Figure 2E). In summary, discrete labeling at native position C31 with Alexa Fluor 488 resulted in active fluorescent RAD51.

Fluorescent RAD51 Filaments Reveal Multiple Nucleations on dsDNA

The functional C319S variant RAD51 labeled at position 31 with Alexa Fluor 488 or Alexa Fluor 555 was incubated with 48 kbp dsDNA (Lambda phage dsDNA, 48,502 bp) at a molar ratio of one RAD51 monomer per 3 bp in the presence of ATP and CaCl_2 (conditions that stabilize RAD51 nucleoprotein filaments; here, no changes observed for >6 hr) (Bugreev and Mazin, 2004; Ristic et al., 2005; van Mameren et al., 2006; data not shown). The resulting DNA-protein complexes were spread on glass microscope slides and observed by epi-fluorescence microscopy (Figure 3A). The averaged contour length of isolated and apparently continuous Alexa Fluor 488-labeled dsDNA filaments was $19.7 \pm 1.1 \mu\text{m}$ ($n = 40$), indicating an average DNA extension of 23% greater than B-form 48 kbp dsDNA. Similar results were obtained with the Alexa Fluor 555-labeled protein; the contour length of filaments was $20.7 \pm 1.4 \mu\text{m}$ ($n = 10$), average DNA extension of 29%. DNA extension by Alexa Fluor-labeled RAD51 on 1.8 kbp DNA measured from SFM images was the same as for unlabeled wild-type RAD51 (38.5% average extension, $n = 7$). This observed RAD51-induced DNA extension was less than the possible maximum 50% extension (Benson et al., 1994; Ristic et al., 2005; van Mameren et al., 2006). This maximum extension was likely not reached due to the relative rates of RAD51 nucleation, extension, and disassociation (T.v.d.H., R. Seidel, M.M., R.K., C.W., and C.D., unpublished data). Using these rates in Monte Carlo simulations of filament formation, saturation with RAD51 on a 48 kbp DNA is predicted to result in maximally $44.84\% \pm 0.015\%$ extension (if nucleation as monomer and filament growth as monomer) or $44.93\% \pm 0.02\%$ extension (if nucleation as pentamer and filament growth as pentamer) ($n = 10$). Because multiple independent RAD51 filaments nucleated on dsDNA are presumably randomly oriented relative to each other, there will be gaps and out of register junctions as they meet due to elongation. This will result in discontinuous protein filaments along DNA and less extension than expected from complete coverage by a single, uninterrupted protein filament.

The predicted filament gaps, even after RAD51 saturation, would not be detectable in fluorescent microscope images. However, limiting the protein concentration should reveal multiple nucleation sites. When 48 kbp dsDNA was incubated with fluorescently labeled RAD51 at a ratio of one monomer per 30 bp and analyzed by epi-fluorescence microscopy as described above, the DNA-bound fluorescent signal appeared in patches (Figure 3B, left panel). From well-isolated strings, 17.7 ± 7 fluorescent patches per dsDNA molecule were detected ($n = 17$), indicating that nucleation occurred at least once every ~2.7 kbp under these conditions. To confirm this interpretation, 48 kbp dsDNA was coated with limiting amount of Alexa Fluor 488-labeled RAD51 (one monomer per 30 bp) after which Alexa Fluor 555-labeled protein was added. The resulting harlequin filaments (Figure 3B, right panel) indicate multiple sites of RAD51 filaments nucleation and show that the dark regions between the

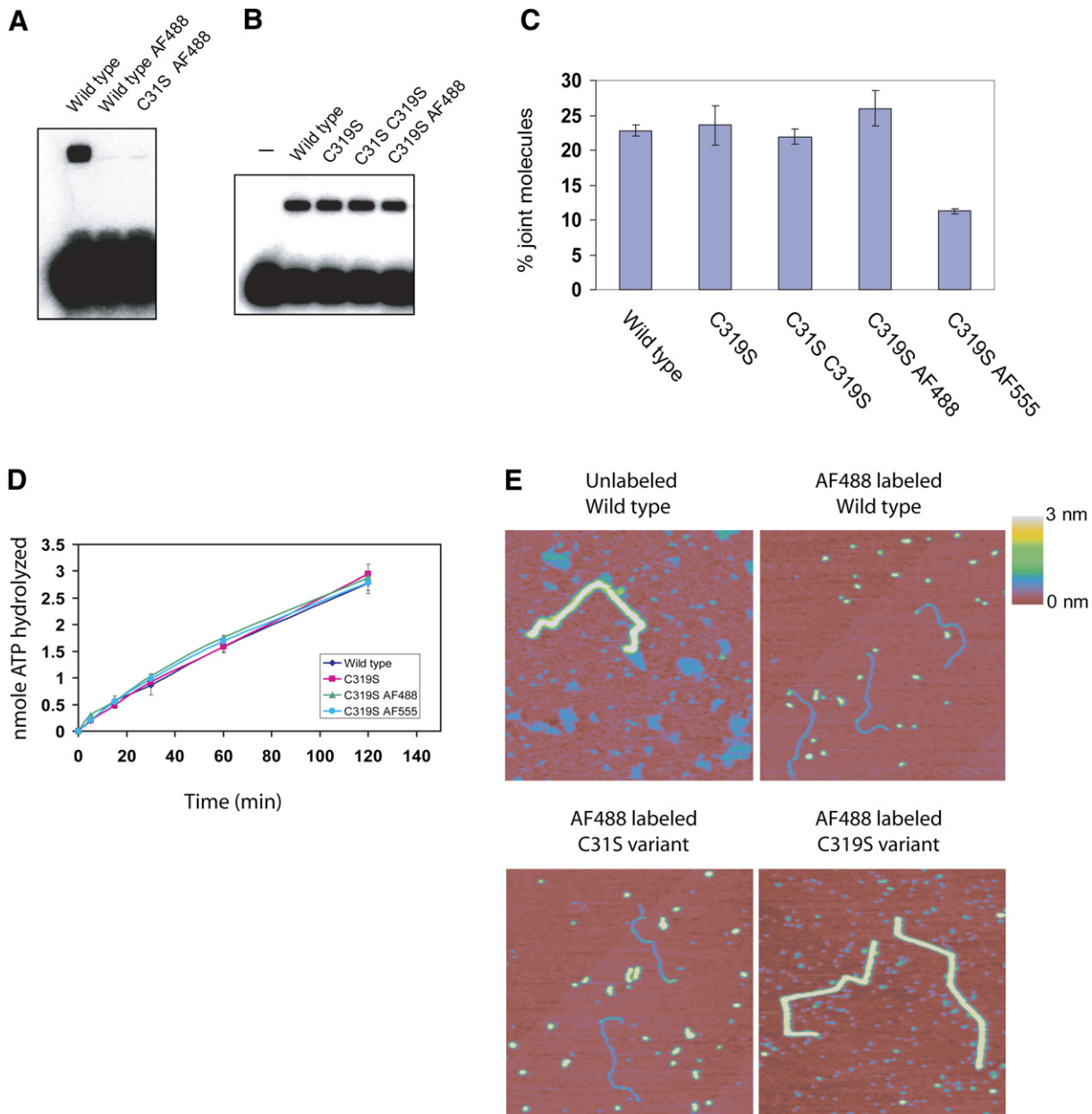


Figure 2. Functional Tests of Alexa Fluor-Labeled RAD51

(A) D-loop activity of unlabeled wild-type, Alexa Fluor 488 (AF488)-labeled wild-type, and C31S RAD51 variant.

(B) Representative gel showing D-loop activity of unlabeled wild-type, C319S, and C31S-C319S RAD51 variants and of Alexa Fluor 488-labeled C319S variant.

(C) Quantification of D-loop activity. Error bars represent standard deviations.

(D) ATPase activity of the various RAD51 variants in the presence of ssDNA. Error bars represent standard deviations.

(E) SFM images of nucleoprotein filament assembled on a 1.8 kb dsDNA substrate in the presence of ATP and CaCl_2 . Similar results were obtained with Alexa Fluor 555-labeled RAD51. Color indicates height (0–3 nm from red to white). Images are $1 \mu\text{m} \times 1 \mu\text{m}$.

fluorescent patches were bare DNA, where additional nucleation occurred when more protein was added. The number of nucleation sites detected by fluorescence microscopy should be considered a lower limit, because small nuclei might be too dim to be detected. Rapid nucleation of RAD51 during nucleoprotein filament formation on dsDNA should also result in evident gaps and multiple

growing points in a time-course analysis where DNA (48 kbp dsDNA) was incubated with Alexa Fluor 488-labeled RAD51 (one monomer per 3 bp) in the presence of ATP and CaCl_2 . After different time intervals, the mixture was spotted on glass and observed by fluorescence microscopy (Figure 3C). One minute after incubation, numerous fluorescent patches representing nucleation sites

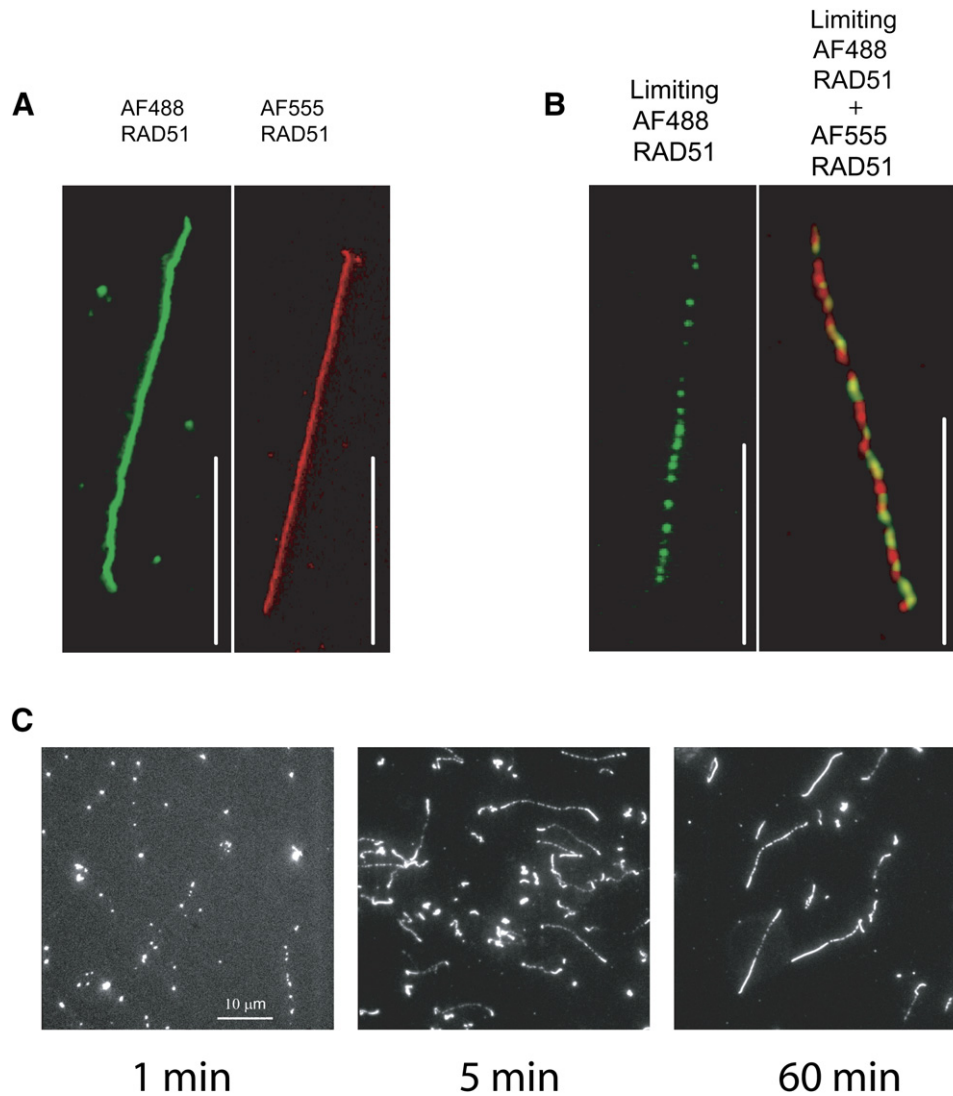


Figure 3. Fluorescent RAD51 Nucleoprotein Filaments on dsDNA

(A) Forty-eight kilo base pairs dsDNA molecule coated with Alexa Fluor 488 (left, AF488)- or Alexa Fluor 555 (right, AF555)-labeled RAD51 at a one monomer/3 bp ratio in the presence of ATP and CaCl_2 and nonspecifically attached to glass.

(B) 48 kbp dsDNA molecule partially coated with RAD51 after incubation with limiting amounts of Alexa Fluor 488-labeled RAD51 in the presence of ATP and CaCl_2 (left panel). Harlequin filament obtained by preincubation of 48 kbp dsDNA with limiting amounts of Alexa Fluor 488-labeled RAD51 followed by incubation with Alexa Fluor 555-labeled RAD51 in the presence of ATP and CaCl_2 (right panel). White bars, 10 μm .

(C) Time-course analysis of filament assembly of Alexa Fluor 488-labeled RAD51 on 48 kbp dsDNA in the presence of ATP and CaCl_2 .

were visible. With time, the fluorescent patches grew and more completely covered the DNA. However, even after incubation for 60 min, most DNA molecules were not fully coated by RAD51. These observations are consistent with filament formation predicted from the nucleation and elongation rates determined in magnetic tweezers experiments (T.v.d.H., R. Seidel, M.M., R.K., C.W., and C.D., unpublished data). These intrinsic properties of RAD51 have made it difficult to experimentally control and monitor the association of RAD51 with dsDNA in real time with our current microscope setup. Rapid RAD51 nucleating was also partially responsible for the inability to analyze nucleation and polymerization phases of RAD51 filament assembly

in a different single molecule assay (Prasad et al., 2006). In contrast, the relatively inefficient nucleation of RecA on dsDNA did allow single-molecule analysis of assembly dynamics for that nucleoprotein filament (Gallego et al., 2006).

If RAD51 nucleates at many sites on a dsDNA molecule, these nascent filaments would grow in random orientations relative to each other (irrespective of the mechanism and polarity of growth). Thus, two stretches of filament growing toward the same point would ultimately collide, likely out of register or with opposite orientations creating a region of discontinuity with one or more bps of bare DNA. Although we could not detect these regions of bare DNA in the fluorescent images, they should be

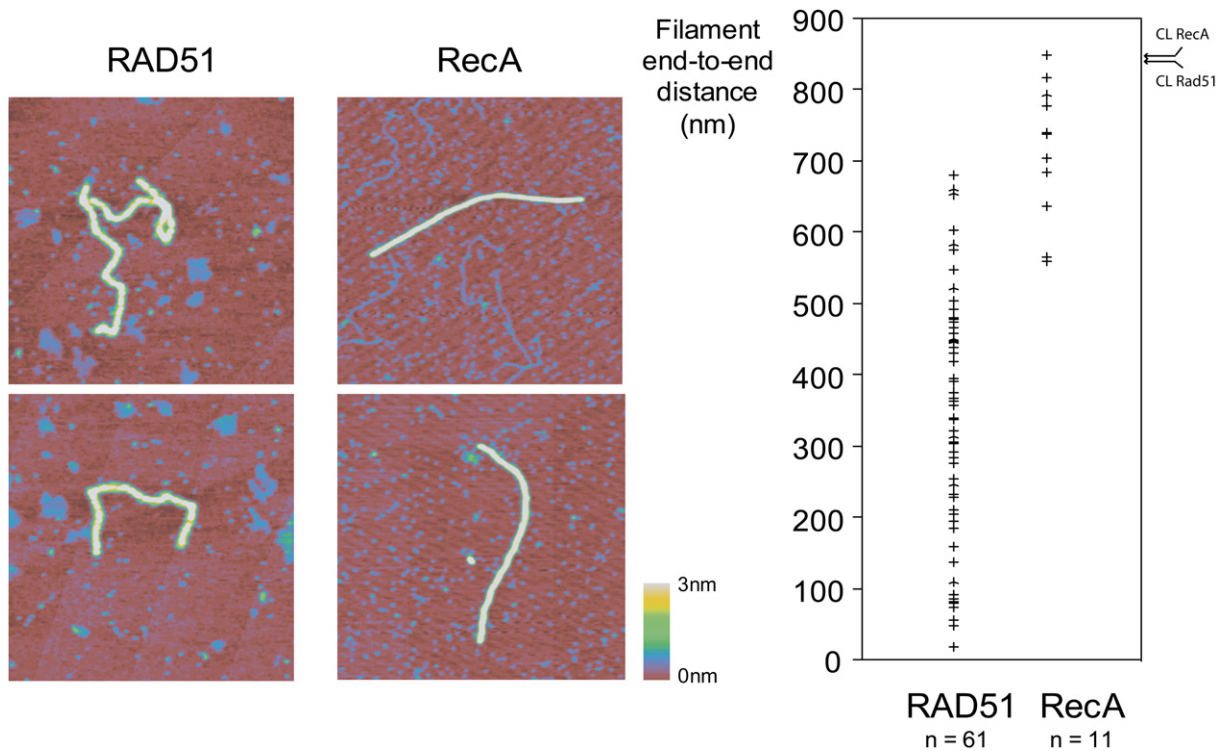


Figure 4. RAD51 Nucleoprotein Filaments on dsDNA Contain Kinks

SFM images of wild-type unlabeled RAD51 nucleoprotein filaments assembled on a 1.8 kbp dsDNA substrate in the presence of ATP and CaCl_2 (left panels) and RecA nucleoprotein filaments assembled on the same DNA substrate in the presence of ATP- γ -S and MgCl_2 (right panels). Images are $1 \mu\text{m} \times 1 \mu\text{m}$. Color indicates height (0–3 nm from red to white). Distribution of filament end-to-end distance is shown on the right. The average contour length was 833 ± 32 nm for RAD51 filaments (CL RAD51) and 841 ± 20 nm for RecA filaments (CL RecA).

more flexible than the adjacent RAD51-coated regions. Indeed in SFM images, RAD51 filaments assembled on a 1.8 kbp dsDNA substrate frequently have kinks representing regions of higher flexibility (Figure 4, left panels). In contrast, kinks were not observed in filaments assembled with RecA on the same DNA substrate (Figure 4), due to the weaker affinity of RecA for dsDNA that results in infrequent nucleation followed by cooperative filament growth (De Zutter and Knight, 1999; McEntee et al., 1981; van der Heijden et al. 2005). To quantify the difference in RAD51 and RecA filaments, we measured their end-to-end distance and contour lengths. The end-to-end distance of RecA nucleoprotein filaments approached the filament contour length (Figure 4), as predicted for a polymer with a persistence length of ~ 900 nm (Hegner et al., 1999). In contrast, the end-to-end distance of the RAD51 filaments deviated substantially from their contour length (Figure 4). From the number of kinks observed in the RAD51 filaments (3.7 ± 1.3 kinks/filament, $n = 61$), we infer that RAD51 nucleated at least once every ~ 500 bp under these conditions. The number of kinks detected by SFM could have been an underestimate because kinks were stringently defined (three points interspersed by 50 nm along the contour length of the filament forming an angle $\geq 70^\circ$). However, this result was confirmed by an independent and unbiased method to estimate the number of RAD51 filaments per DNA molecule. We calculated the

Kuhn segment length l , assuming that the separate, stiff filaments along the DNA contour comprise the links of a freely jointed chain, to be 169 nm (by using $l = R^2/L$ where R is the end-to-end distance [375 nm] and L the contour length [833 nm]). This yielded approximately four freely jointed chain hinges or kinks per filament, in agreement with the number determined from direct observation described above. Both the fluorescent and SFM images indicate that RAD51 filaments assembled on dsDNA were discontinuous. The importance of mediator proteins such as BRCA2, which has been implicated in targeting RAD51 specifically to a ds/ssDNA transition, may be to control filament nucleation in order to avoid discontinuities and filament segments with opposite orientation (Sung, 2005; Yang et al., 2005).

Dynamic RAD51 Nucleoprotein Filament Disassociation

Fluorescent RAD51 allowed us to describe nucleoprotein filaments dynamics in solution in real time. Filaments, formed by incubating 48 kbp dsDNA molecules biotinylated at one end with Alexa Fluor 488-labeled RAD51 in the presence of ATP and CaCl_2 , were tethered to a surface, extended by buffer flow and observed in a fluorescent microscope. Movie S1, available with this article online, shows a single surface-tethered DNA molecule coated with fluorescent RAD51 stretched by buffer flow

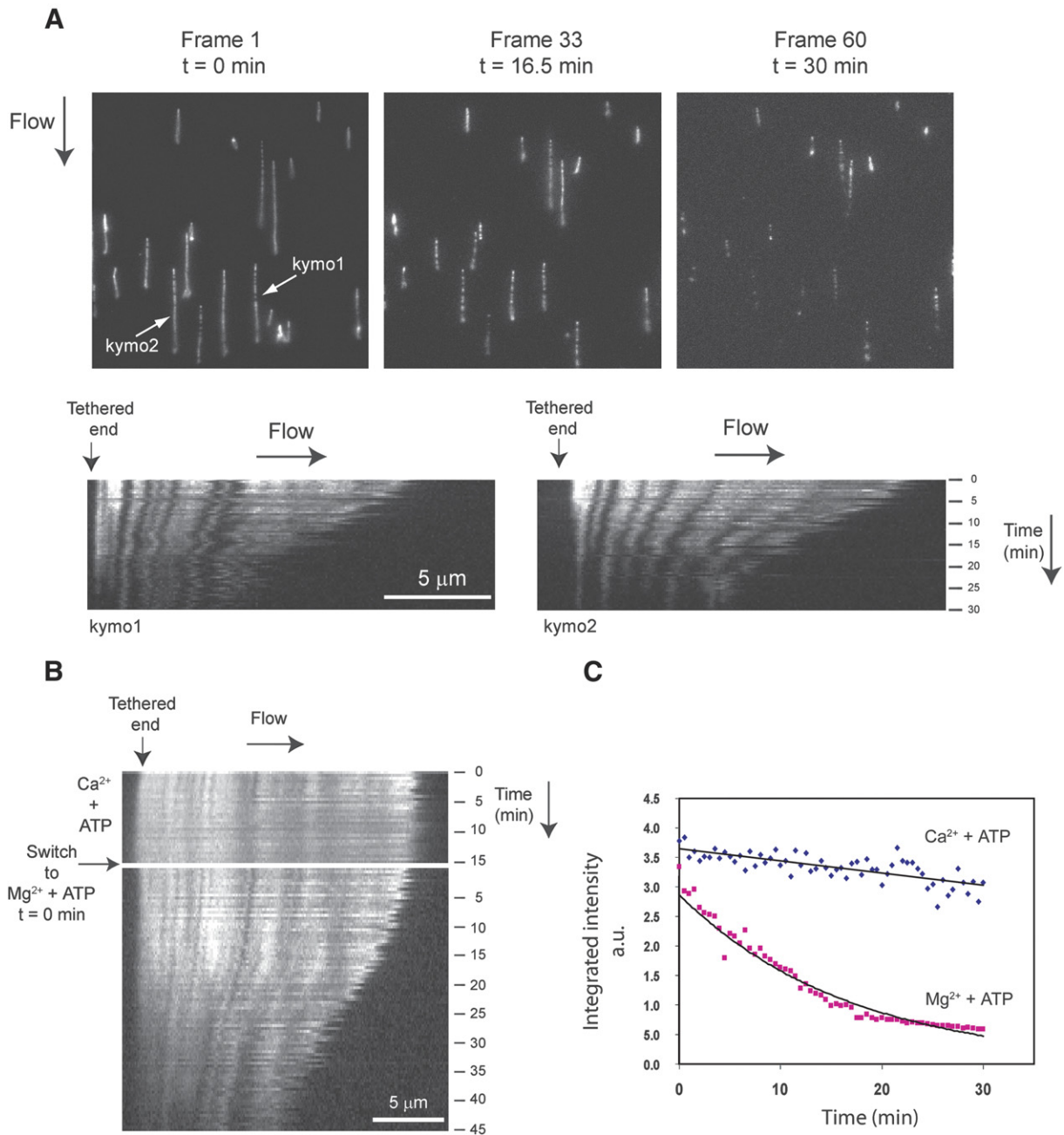


Figure 5. Visualization of Fluorescent RAD51 Nucleoprotein Filaments in Buffer

Constructs were assembled by incubation of one-end biotinylated 48 kbp dsDNA molecules with Alexa Fluor 488-labeled C319S RAD51 in the presence of ATP and CaCl₂ and tethered on streptavidin-coated glass (see [Experimental Procedures](#)). (A) Immediately after capture, the constructs were extended by applying hydrodynamic flow with a buffer containing MgCl₂ and ATP to trigger ATP hydrolysis. Disassociation was recorded by time-lapse CCD imaging. Frames 1, 33, and 60 of the time-lapse movie (see [Movie S3](#)) are displayed with the direction of the buffer flow indicated. Kymographs for two individual constructs (kymo1 and kymo2) are presented on the bottom. The tethered end corresponds to the fixed end of the construct that is attached to the glass. (B) Kymograph from a time-lapse movie showing the behavior of a construct under CaCl₂/ATP conditions for 15 min (top) and for 45 min after switching to MgCl₂/ATP conditions (bottom). (C) Representative plot of the disassociation of Alexa Fluor 488-labeled RAD51 from a 48 kbp dsDNA molecule. Disassociation in presence of MgCl₂/ATP (red, bold line: fit to first order exponential decay) or CaCl₂/ATP (blue, bold line: fit to linear regression).

alternating in forward and reverse direction. Fluorescent filaments tethered to the surface via one end and observed in flow have a patchy appearance, again indicating

multiple nucleation events ([Movie S1](#), [Figure 5A](#), frame 1, and associated [Movie S3](#)). Functional RAD51 filament dynamics could now be directly observed and analyzed in

real time in controlled conditions. In CaCl_2 -containing buffers, where ATP hydrolysis by RAD51 is greatly suppressed (Bugreev and Mazin, 2004), the relative position and length of fluorescent patches interspersed by dark gaps did not appreciably change over time (e.g., Figure 5B, upper panel, and Movie S2). This indicated that filament segments were tightly associated with DNA and did not diffuse or slide along DNA molecules.

Mechanistically important changes in the arrangement and architecture of RAD51 filaments are expected to occur when ATP is hydrolyzed. By replacing CaCl_2 with MgCl_2 in the flowing buffer, ATP hydrolysis was activated, controllably triggering filament shrinkage/disassembly (Figure 5A and Movie S3). Examples of single filaments followed over time are presented as kymographs (Figure 5A, lower panels kymo1 and kymo2, and Figure 5B). This loss of fluorescence accompanied by a decrease in length clearly indicated disassociation of fluorescent protein and disassembly of filament segments. The disassembly followed here additionally indicated that fluorescent protein in these filaments maintained biochemical function. Thus, the lack of filament diffusion or sliding, noted above, was not due to a loss of biochemical activity.

The rate of RAD51 disassociation was determined by following the integrated fluorescence intensity in time along seven full constructs and four continuous fluorescent patches (see representative plot in Figure 5C). The resulting fluorescence loss curves were fit to a single exponential decay (Figure 5C) giving average time constants of 12.48 ± 3.00 min and 11.77 ± 0.50 min, for the full constructs and the individual patches, respectively. Assuming disassociation from one end, Monte Carlo simulation of these data give a disassociation rates of $0.022 \pm 0.005 \text{ s}^{-1}$ per end and $0.020 \pm 0.001 \text{ s}^{-1}$ per end, for whole constructs and filament patches, respectively, very similar to the rate of RAD51 disassociation determined in single-molecule magnetic tweezers experiments ($0.021 \pm 0.001 \text{ s}^{-1}$ per end) (T.v.d.H., R. Seidel, M.M., R.K., C.W., and C.D., unpublished data).

All of our observations indicate that RAD51 nucleates avidly on dsDNA *in vitro*. RAD51 thus has the potential to bind to and assemble filaments on dsDNA sites that are not necessarily substrates for homologous recombination activity. *In vivo*, this would have deleterious effects such as undesired reactions at these sites or unnecessary sequestering of RAD51 in nonfunctional complexes. Thus, disassembly of RAD51 filaments from dsDNA would be needed to counteract unproductive binding. Here, we have observed RAD51 disassembly by loss of fluorescent protein and determined this occurs with an intrinsic rate of 0.02 monomers per second when ATP hydrolysis is activated. The same rate was determined for disassembly from dsDNA followed by decrease in DNA length in magnetic tweezers (T.v.d.H., R. Seidel, M.M., R.K., C.W., and C.D., unpublished data). Disassembling filaments from the dsDNA products of strand exchange is also a required step in recombination, functioning possibly to drive the reaction forward and certainly needed to allow other proteins access to the DNA structures created by strand

exchange. *In vivo* disassembly of RAD51 filaments would be important both at sites inappropriately assembled on dsDNA or those present after joint molecule formation. The recombination factors Rad54, Rad54B, and Tid1 likely facilitate RAD51 disassociation from dsDNA and may specifically increase the rate of RAD51 disassociation (Holzen et al., 2006; Solinger et al., 2002; Sung and Klein, 2006; Symington and Heyer, 2006; Wesoly et al., 2006).

The visualization of RAD51 nucleoprotein filaments in solution that we presented here revealed patches of filament and bare DNA, indicating multiple nucleation events. The resulting discontinuities explain some features of RAD51 filaments observed here and elsewhere (Ristic et al., 2005); less than 50% extension, the presence of kinks, and the related variation in contour length and Kuhn segment length of filaments. We have also demonstrated that this fluorescent RAD51 forms filaments indistinguishable from unlabeled protein and that these did not slide along DNA. The previously reported passive and ATP hydrolysis independent sliding of RAD51 complexes along dsDNA (Granéli et al., 2006b) is not a characteristic of RAD51 assembled into filaments. This, and similar observations from other single-molecule analyses of these fluorescent RAD51 filaments (van Mameren et al., 2006), strongly suggested that functional RAD51 filament segments are tightly associated with DNA when ATP hydrolysis is inhibited. Filament disassembly occurred when ATP hydrolysis was activated. The same rate was determined here by observing the protein as we have also determined in magnetic tweezers by following changes in DNA length.

The emerging picture of RAD51 nucleoprotein filaments includes patches of proteins filaments interspersed with bare DNA in a dynamic arrangement resulting from the continuous interplay of nucleation, elongation, and disassembly. These intrinsic aspects of RAD51-DNA interactions define the baseline activities likely targeted for influence by recombination mediators.

EXPERIMENTAL PROCEDURES

Protein Production

Wild-type and variants of human RAD51 were all purified by the same procedure. The human RAD51 open reading frame with a NcoI site encompassing the ATG and a BamHI site just after the stop codon was subcloned between the NcoI and BamHI sites of pET11d (Novagen). The cysteine-to-serine variants were generated by the QuikChange Site-Directed Mutagenesis method by using the wild-type RAD51 pET11d subclone as template (Stratagene). Overexpression was performed in 12 l batches in Rosetta/pLysS or Rosetta2/pLysS cells (Novagen) by pregrowth at 37°C until the $\text{OD}_{600\text{nm}}$ reached 0.5 followed by induction at the same temperature for 4 hr after addition of IPTG to 0.5 mM. Cells were collected by centrifugation and resuspended with 36 ml of PBS giving ~80 ml of cell paste that was frozen at -80°C . Lysis was performed by addition of one volume of 3 M NaCl, 100 mM Tris-HCl (pH 7.5), 4 mM EDTA, 20 mM β -mercaptoethanol, 2 mM PMSF/isopropanol to the thawed cell paste. The lysate was briefly sonicated and clarified by centrifugation at 20,000 rpm at 4°C in a Sorval SS34 rotor. Polyethylenimine (10% stock [pH 7.5] with HCl) was added drop by drop while mixing to the decanted supernatant to a final concentration of 0.1% and incubated on ice for >1 hr. After clarification as described above, one volume of 4 M $(\text{NH}_4)_2\text{SO}_4$ was slowly added while mixing to the decanted supernatant and incubated

for >1 hr on ice. The precipitate containing RAD51 was collected by centrifugation at 10,000 rpm in a GSA Sorval rotor for 30 min at 4°C, resuspended in 0.5 M KCl, 50 mM Tris-HCl (pH 7.5), 1 mM EDTA, 2 mM DTT, 10% glycerol and clarified by centrifugation at 20,000 rpm at 4°C in a Sorval SS34 rotor. After dialysis against 0.15 M KCl, 50 mM Tris-HCl (pH 7.5), 1 mM EDTA, 2 mM DTT, and 10% glycerol, the sample was loaded on a 5 ml heparin sepharose column equilibrated in the same buffer. A KCl gradient from 0.15 to 0.6 M was applied to the column. RAD51 eluted around 400 mM KCl. Peak fractions were pooled, diluted 3-fold with 50 mM Tris-HCl (pH 7.5), 1 mM EDTA, 2 mM DTT, and 10% glycerol, and loaded on a 1 ml MonoQ column equilibrated with 0.15 M KCl, 50 mM Tris-HCl (pH 7.5), 1 mM EDTA, 2 mM DTT, and 10% glycerol. RAD51 eluted around 300 mM KCl in a gradient from 0.15 to 0.6 M KCl. Pooled peak fractions were aliquoted and stored at -80°C.

Protein Labeling

Just prior to use, the concentration of DTT was adjusted to 20 mM in the above-described samples (at 1–2 mg/ml of RAD51) and incubated for 30 min on ice. The sample was buffer exchanged (EconoPac 10DG, BIORAD) into labeling buffer (50 mM MOPS-HCl [pH 7.0], 300 mM KCl, 1 mM EDTA, 10% glycerol, degassed with argon for 30 min prior to use). The maleimide-coupled dye (Molecular Probes) was resuspended in labeling buffer just prior to use and immediately added to the protein sample at a 10-fold molar excess (dye/protein) while mixing. The reaction was incubated on ice for 30 min and quenched by addition of DTT to 20 mM with further 30 min incubation on ice. Excess dye was removed by buffer exchange into 0.3 M KCl, 50 mM Tris-HCl (pH 7.5), 1 mM EDTA, 2 mM DTT, 10% glycerol as described above and dialyzed against the same buffer before storage at -80°C.

Mass Spectrometry

Protein samples were first desalted with a ZipTip_{C4} pipette tip (Millipore). The tip was wet with acetonitrile and equilibrated with 0.1% trifluoroacetic acid in Milli-Q water. After adsorption of the protein sample, the tip was washed with 0.1% trifluoroacetic acid in Milli-Q water and finally eluted with 0.1% trifluoroacetic acid in 50% acetonitrile. One volume of the eluate was mixed with one volume of a sinapinic matrix solution (3.4 mg sinapinic acid in 30% acetonitrile) and deposited on a stainless-steel plate for analysis by mass spectrometry. A Biflex III mass spectrometer driven by FLEXcontrol and FLEXanalysis v2.0 software (Bruker Daltonics) was used. Control experiments where the labeled and unlabeled proteins were premixed at known ratios showed that the presence of the dye did not influence ionization of the protein.

ATPase Assays

Reactions (60 μ l) contained 50 μ M virion ϕ X174 DNA (NEB), 2.5 μ M recombinase in 50 mM Tris (pH 7.5), 2 mM DTT, 2 mM MgCl₂, 100 μ g/ml acetylated BSA, 0.2 mM ATP, and 83 nM [γ -³²P]ATP (6000 Ci/mmol, 10 mCi/ml). Incubation was at 37°C, and at the indicated times, 5 μ l aliquots were removed, stopped by addition of 5 μ l of 0.5 M EDTA, and analyzed by thin-layer chromatography (PEI-cellulose-F) with 0.4 M LiCl and 1 M formic acid as running buffer. Plates were air-dried, and signals were captured by Phosphorimaging with a Typhoon scanner and quantified with ImageQuant version 5.2 (Molecular Dynamics).

D-Loop Assays

Reactions were performed in a final volume of 20 μ l containing either 5'-end radiolabeled SK3 oligonucleotide (Mazin et al., 2000) at 3.6 μ M (nucleotides), 1.6 μ M RAD51, 50 mM Tris-HCl (pH 7.5), 1 mM DTT, 0.1 mg/ml acetylated BSA, 60 mM KCl, 2 mM CaCl₂, and 1 mM ATP (Bugreev and Mazin, 2004). After 5 min incubation at 37°C, 5 μ l of supercoiled pUC19 plasmid DNA at 0.38 mg/ml (prepared by detergent lysis and purified twice by CsCl gradient equilibrium sedimentation) was added and further incubated for 20 min at 37°C. Reactions were stopped by addition of 5 μ l of 0.5% SDS, 50 mM EDTA, and

30% glycerol and deproteinized by incubation for 5 min at 37°C with 1 μ g/ μ l final of Proteinase K. Reaction mixtures were fractionated by 0.6% agarose gel electrophoresis in Tris-Borate buffer. Gels were dried on DEAE paper, and signals were captured by Phosphorimaging with a Typhoon scanner and quantified with ImageQuant version 5.2 (Molecular Dynamics).

Scanning Force Microscopy Analysis

The dsDNA used in the SFM experiments was made by linearization of pDER11 (Ristic et al., 2001) with Scal, producing 1821 bp blunt-end linear dsDNA, which was deproteinized by phenol:chloroform:iso-amyl alcohol (25:24:1) extraction. RAD51 nucleoprotein filaments were formed in 10 μ l reaction volume containing 7.5 μ M DNA (bp), 2.5 μ M RAD51, 25 mM HEPES-KOH (pH 7.5), 5 mM CaCl₂, 2 mM ATP, and 30 mM KCl. Reactions were carried out at 37°C for 1 hr and then placed on ice. Nucleoprotein filaments of RecA were produced in 10 μ l reaction volume containing 7.5 μ M DNA (bp), 2.5 μ M RecA, 25 mM HEPES-KOH (pH 7.0), 10 mM MgCl₂, 2 mM ATP- γ -S, and 30 mM KCl. Reactions were carried out at 37°C for 1 hr and then placed on ice. For imaging, reaction mixtures were diluted 15-fold in deposition buffer (10 mM HEPES-KOH [pH 7.5], 10 mM MgCl₂) and deposited on freshly cleaved mica. After about 30 s, the mica was washed with water (glass distilled; SIGMA) and exposed to a stream of filtered air. Images were obtained on a NanoScope IIIa and a NanoScope IV (Veeco; Santa Barbara, CA) operating in tapping mode in air with a type E scanner. Silicon nanotips were purchased from Veeco. Contour lengths, end-to-end distances, and angles were measured with ImageJ 1.33u (<http://rsb.info.nih.gov/ij>).

Assembly and Visualization of Static Fluorescent Filaments Deposited on Glass

Filaments were assembled in a 50 μ l reaction mixture containing 64 pM (molecules) of Lambda phage dsDNA (NEB, after end filling with Klenow exo⁻), 1 μ M RAD51, 50 mM Tris-HCl (pH 7.5), 1 mM ATP, 2 mM CaCl₂, 1 mM DTT, 0.1 mg/ml BSA, and 60 mM KCl. After 60 min incubation at 37°C, the reaction mixture was diluted by addition of 1 ml of Milli-Q water. Aliquots were immediately deposited and spread on glass microscope slides (superfrost from Menzel-Glaser) with a contact time of ~2 min. The slides were washed with gentle stream of Milli-Q water, drained and mounted in Vectashield (Vector Laboratories). Filaments in Figure 3 were observed by epi-fluorescence with Leitz 63 \times (NA 1.40) or 100 \times (NA 1.32) oil-immersion objectives with an Aristoplan Leitz microscope and a DXC-950P Power HAD 3CCD color camera (Sony). Images were acquired with either single-band pass or double-band pass filters. Contour lengths were measured with ImageJ 1.33u.

Surface Tethering and Visualization of Fluorescent Filaments in Buffer

Lambda phage dsDNA was biotinylated at one (left) end by Klenow exo⁻ end-filling reaction in the presence of biotin-21-dUTP (BD Biosciences), dATP, and dGTP, followed by an ethanol precipitation step. The sample was subjected to a second end-filling reaction but this time in the presence of the four standard dNTPs to create blunt ends. Alternatively, biotinylation of phage Lambda DNA ends was performed by annealing biotinylated oligonucleotides complementary to the cos ends as described (Granéli et al., 2006a). Filaments were assembled as described above, diluted in CaCl₂/ATP assembly buffer, and injected in a flow cell prepared as follows. Extravidin (Sigma) was introduced in a flow cell (#1 glass coverslip, Menzel-Glaser) at 1 mg/ml and allowed to interact for 30 min. After removal of excess Extravidin, the flow cell was washed and blocked with 2 mg/ml acetylated BSA, 2 mg/ml α -casein, 100 μ g/ml catalase, 400 μ g/ml glucose oxidase, 50 μ g/ml glucose, 10 mM DTT, 50 mM Tris-HCl (pH 7.5), 30 mM KCl, and 10% glycerol. Hydrodynamic flow was controlled with a precision pump (Harvard Apparatus). Dynamic visualization of filaments was performed with a Nikon 60 \times or 100 \times (NA 1.45) TIRF objective by using a Nikon TE2000U inverted microscope equipped with a Cascade 512B

CCD camera (Princeton Instruments) and driven with Metamorph (Molecular Devices). Excitation was performed either with a mercury lamp or by using the 488 nm line of a 40 mW argon laser. Kymographs were generated by the kymograph Metamorph software routine and obtained by averaging the intensity over 20 pixels orthogonal to the construct contour length.

Monte Carlo Simulations

The binding of hRAD51 onto a DNA substrate was modeled by using Monte Carlo simulations. A one-dimensional array was used to mimic the DNA substrate containing a number of elements equivalent to the number of base pairs (48,000) of the DNA molecule of interest. RAD51 filament assembly was described by nucleation followed by growth that extended the nucleation point with rates as determined (T.v.d.H., R. Seidel, M.M., R.K., C.W., and C.D., unpublished data). Upon binding of hRAD51 to the DNA substrate, the protein was assumed to cover $5 \times 3 = 15$ nucleotides or base pairs and to elongate the binding-site length to a value corresponding to 50% compared to the base-base spacing in dsDNA (Ogawa et al., 1993; Sung and Robberson, 1995).

After saturation of filament assembly, disassembly was triggered. A monomer located at the end of a filament opposite to the filament extension end (i.e., toward lower numbers in the array) was allowed to dissociate. A value was randomly extracted from a uniform distribution yielding a value between 0 and 1. If this value was smaller than the threshold set by the disassociation rate, the monomer dissociated, and a vacancy was created. This threshold value, which is a rate expressed in $(\text{Monte Carlo step})^{-1}$, converts into a kinetic rate expressed in s^{-1} when the ratio between a Monte Carlo step and the time dependence of the data is obtained after fitting. A full description of the simulation method will be given elsewhere (T.v.d.H., R. Seidel, M.M., R.K., C.W., and C.D., unpublished data).

Supplemental Data

Supplemental Data include three movies and are available at <http://www.structure.org/cgi/content/full/15/5/599/DC1/>.

ACKNOWLEDGMENTS

We thank Theo Luider for advice with mass spectrometry, Murray Junop for generating the 3D model of human RAD51, Dubi Drabek for the gift of the human RAD51 cDNA, and André Eker for critical reading of the manuscript. This work was supported by grants from the Dutch Cancer Society (KWF), the Netherlands Organization for Scientific Research (NWO), the Dutch Foundation for Fundamental Research of Matter (FOM), the Association for International Cancer Research (AICR), and the European Commission (IP 512113).

Received: July 25, 2006

Revised: March 28, 2007

Accepted: April 13, 2007

Published: May 15, 2007

REFERENCES

- Bates, P.A., and Sternberg, M.J. (1999). Model building by comparison at CASP3: using expert knowledge and computer automation. *Proteins (Suppl 3)*, 47–54.
- Bates, P.A., Kelley, L.A., MacCallum, R.M., and Sternberg, M.J. (2001). Enhancement of protein modeling by human intervention in applying the automatic programs 3D-JIGSAW and 3D-PSSM. *Proteins Suppl.* 5, 39–46.
- Benson, F.E., Stasiak, A., and West, S.C. (1994). Purification and characterization of the human RAD51 protein, an analogue of *E. coli* RecA. *EMBO J.* 13, 5764–5771.
- Bugreev, D.V., and Mazin, A.V. (2004). Ca^{2+} activates human homologous recombination protein Rad51 by modulating its ATPase activity. *Proc. Natl. Acad. Sci. USA* 101, 9988–9993.
- Contreras-Moreira, B., and Bates, P.A. (2002). Domain fishing: a first step in protein comparative modelling. *Bioinformatics* 18, 1141–1142.
- Conway, A.B., Lynch, T.W., Zhang, Y., Fortin, G.S., Fung, C.W., Symington, L.S., and Rice, P.A. (2004). Crystal structure of a Rad51 filament. *Nat. Struct. Mol. Biol.* 11, 791–796.
- De Zutter, J.K., and Knight, K.L. (1999). The hRad51 and RecA proteins show significant differences in cooperative binding to single-stranded DNA. *J. Mol. Biol.* 293, 769–780.
- Galletto, R., Amitani, I., Baskin, R.J., and Kowalczykowski, S.C. (2006). Direct observation of individual RecA filaments assembling on single DNA molecules. *Nature* 443, 875–878.
- Granéli, A., Yeykal, C.C., Prasad, T.K., and Greene, E.C. (2006a). Organized arrays of individual DNA molecules tethered to supported lipid bilayers. *Langmuir* 22, 292–299.
- Granéli, A., Yeykal, C.C., Robertson, R.B., and Greene, E.C. (2006b). Long-distance lateral diffusion of human Rad51 on double-stranded DNA. *Proc. Natl. Acad. Sci. USA* 103, 1221–1226.
- Hegner, M., Smith, S.B., and Bustamante, C. (1999). Polymerization and mechanical properties of single RecA-DNA filaments. *Proc. Natl. Acad. Sci. USA* 96, 10109–10114.
- Holzen, T.M., Shah, P.P., Olivares, H.A., and Bishop, D.K. (2006). Tid1/Rdh54 promotes disassociation of Dmc1 from nonrecombinogenic sites on meiotic chromatin. *Genes Dev.* 20, 2593–2604.
- Lauder, S.D., and Kowalczykowski, S.C. (1991). Asymmetry in the recA protein-DNA filament. *J. Biol. Chem.* 266, 5450–5458.
- Mazin, A.V., Zaitseva, E., Sung, P., and Kowalczykowski, S.C. (2000). Tailed duplex DNA is the preferred substrate for Rad51 protein-mediated homologous pairing. *EMBO J.* 19, 1148–1156.
- McEntee, K., Weinstock, G.M., and Lehman, I.R. (1981). Binding of the recA protein of *Escherichia coli* to single- and double-stranded DNA. *J. Biol. Chem.* 256, 8835–8844.
- Ogawa, T., Yu, X., Shinohara, A., and Egelman, E.H. (1993). Similarity of the yeast RAD51 filament to the bacterial RecA filament. *Science* 259, 1896–1899.
- Prasad, T.K., Yeykal, C.C., and Greene, E.C. (2006). Visualizing the assembly of human Rad51 filaments on double-stranded DNA. *J. Mol. Biol.* 363, 713–728.
- Ristic, D., Wyman, C., Paulusma, C., and Kanaar, R. (2001). The architecture of the human Rad54-DNA complex provides evidence for protein translocation along DNA. *Proc. Natl. Acad. Sci. USA* 98, 8454–8460.
- Ristic, D., Modesti, M., van der Heijden, T., van Noort, J., Dekker, C., Kanaar, R., and Wyman, C. (2005). Human Rad51 filaments on double- and single-stranded DNA: correlating regular and irregular forms with recombination function. *Nucleic Acids Res.* 33, 3292–3302.
- Shan, Q., and Cox, M.M. (1996). RecA protein dynamics in the interior of RecA nucleoprotein filaments. *J. Mol. Biol.* 257, 756–774.
- Shan, Q., and Cox, M.M. (1997). RecA filament dynamics during DNA strand exchange reactions. *J. Biol. Chem.* 272, 11063–11073.
- Solinger, J.A., Kiianitsa, K., and Heyer, W.D. (2002). Rad54, a Swi2/Snf2-like recombinational repair protein, disassembles RAD51:dsDNA filaments. *Mol. Cell* 10, 1175–1188.
- Sung, P. (2005). Mediating repair. *Nat. Struct. Mol. Biol.* 12, 213–214.
- Sung, P., and Robberson, D.L. (1995). DNA strand exchange mediated by a RAD51-ssDNA nucleoprotein filament with polarity opposite to that of RecA. *Cell* 82, 453–461.
- Sung, P., and Klein, H. (2006). Mechanism of homologous recombination: mediators and helicases take on regulatory functions. *Nat. Rev. Mol. Cell Biol.* 7, 739–750.

Symington, L.S., and Heyer, W.D. (2006). Some disassembly required: role of DNA translocases in the disruption of recombination intermediates and dead-end complexes. *Genes Dev.* *20*, 2479–2486.

van der Heijden, T., van Noort, J., van Leest, H., Kanaar, R., Wyman, C., Dekker, N.H., and Dekker, C. (2005). Torque-limited RecA polymerization on dsDNA. *Nucleic Acids Res.* *33*, 2099–2105.

van Mameren, J., Modesti, M., Kanaar, R., Wyman, C., Wuite, G.J., and Peterman, E.J. (2006). Dissecting elastic heterogeneity along DNA molecules coated partly with Rad51 using concurrent fluorescence microscopy and optical tweezers. *Biophys. J.* *91*, L78–L80.

Wesoly, J., Agarwal, S., Sigurdsson, S., Bussen, W., Van Komen, S., Qin, J., van Steeg, H., van Bentham, J., Wassenaar, E., Baarends,

W.M., et al. (2006). Differential contributions of mammalian Rad54 paralogs to recombination, DNA damage repair, and meiosis. *Mol. Cell. Biol.* *26*, 976–989.

Wu, Y., He, Y., Moya, I.A., Qian, X., and Luo, Y. (2004). Crystal structure of archaeal recombinase RADA: a snapshot of its extended conformation. *Mol. Cell* *15*, 423–435.

Yang, H., Li, Q., Fan, J., Holloman, W.K., and Pavletich, N.P. (2005). The BRCA2 homologue Brh2 nucleates RAD51 filament formation at a dsDNA-ssDNA junction. *Nature* *433*, 653–657.

Yu, X., Jacobs, S.A., West, S.C., Ogawa, T., and Egelman, E.H. (2001). Domain structure and dynamics in the helical filaments formed by RecA and Rad51 on DNA. *Proc. Natl. Acad. Sci. USA* *98*, 8419–8424.